

Optical switching in graded plasmonic waveguides

J. J. Xiao

*Department of Physics, The Chinese University of Hong Kong,
Shatin, New Territories, Hong Kong, China*

K. Yakubo

*Division of Applied Physics, Graduate School of Engineering,
Hokkaido University, N13-W8, Sapporo 060-8628, Japan*

K. W. Yu*

*Department of Physics and Institute of Theoretical Physics,
The Chinese University of Hong Kong,
Shatin, New Territories, Hong Kong, China*

(Dated: February 6, 2008)

Abstract

A new mechanism of longitudinal confinement of optical energy via coupled plasmon modes is proposed in chains of noble metal nanoparticles embedded in a graded dielectric medium, which is analogous to the confinement of electrons in semiconductor quantum wells. In these systems, one can control the transmission of optical energy by varying the graded refractive index of the host medium or the separation between the nanoparticles to realize the photonic analogue of electronic transistors. Possible passband tunability by nanoparticle spacing and modulation of the refractive index in the host medium have been presented explicitly and compared favorably with numerical calculations.

PACS numbers: 78.67.-n, 73.20.Mf, 42.79.Gn, 78.67.Bf

* Electronic address: kwyu@phy.cuhk.edu.hk

One of the most attractive studies in advanced optics is to conquer the general difficulties in conventional photonics: (1) restriction of the diffraction limit, which prevents achieving high degree of miniaturization and monolithic integration of optical devices and circuits; and (2) light fields existing in three dimensions, inhibiting integrated on-chip devices. A prominent way to overcome these two major obstacles is related to use of surface plasmons (SPs) in plasmonic structures, e.g., see Refs. 1-8 and references cited therein. Along with the advancement of nanofabrication techniques, many nanostructures and devices based on SPs have been studied, for example, metallic nanoparticles,⁵ nanowires,² nanostrips,⁴ and metal grooves⁹ and wedges,¹⁰ as well as integrated components such as nanoparticle chains,⁸ multilayers,¹¹ and combined plasmonic and dielectric waveguides.¹² They essentially utilize SPs features of *lateral/transverse* localization and evanescence,¹³ and their operations in near-field regime, thus can easily beat the above mentioned restrictions in conventional photonics.

Although these plasmonic systems offer the advantages to relieve the difficulties in the miniaturization and integration of photonic devices, SPs suffer from intrinsic dissipation of consisted material, e.g., mostly noble metals like gold and silver and thus decay excessively along the propagation direction, or referred to the longitudinal direction. Nevertheless, their propagation length is still satisfactory in nanooptics, e.g., $1/e$ propagation lengths of a few tens of μm are reported.¹⁴ It is, alternatively, desirable to have localized SPs in the longitudinal direction, in addition to their naturally lateral/transverse confinement. In this sense, they may sustain modes in ultrasmall volume and highly confined electromagnetic field. To this end, only very few works have focused on this issue, for instance, nano-concentration of optical energy by localizing SPs in graded plasmonic waveguides (i.e., axially nonuniform waveguides),¹⁵ and symmetry breaking in plasmonic chains, which helps the enhancement of local fields, and facilitates the forming of localization of SPs due to asymmetric polarization charge distribution.¹⁶ Other examples include using nanoscale Fabry-Pérot cavity to confine SPs inside,¹⁷ and constructing plasmonic crystals by decorating or structuring metallic surfaces at nanoscale.^{3,18} In analogy of photonic crystals, coupled SPs show localization near the band-edges in these plasmonic crystals and demonstrate desirable localizations.

In this work, we show that precise control of *longitudinal localization* of SPs in plasmonic nanoparticle chains (PNCs) is possible by simply imposing a gradient in the refractive indices of the surrounding host medium, which can behave like a plasmonic switcher. The localization mechanism is different from those of the two extreme cases: periodically structured plasmonic

crystals^{3,19,20} and disordered plasmonic systems.^{21,22} In fact, closely-separated PNCs were proposed for potential applications in energy guiding and routing inside the subwavelength scale.⁸ Also they were demonstrated efficiently converting propagating light (far-fields) to SPs (near-fields).²³ The precise control of SPs in our proposed system can also achieve confinement of electromagnetic fields in specific region to control their interactions with specimen.²⁴ Furthermore, we can envision applications of such PNC arrays that evanescently couple two dielectric slab waveguides, e.g., in photo-addressable birefringent polymer matrix (optical control) or in electro-optical materials such as liquid crystals (electrical control).

Let us assume that a chain of N identical metallic nanoparticles of Drude form dielectric function $\epsilon_m(\omega) = 1 - \omega_p^2/\omega^2$ (lossless) is immersed in a dielectric host with its dielectric function varying from the left-hand side to the right-hand side along x -axis as

$$\epsilon_2(x) = \epsilon_{\text{left}} + cx/l, \quad (1)$$

where x denotes the position of the particles, l the total length of the chain, and c the coefficient of dielectric gradient which can be formed naturally, induced by a pump light that possesses intensity variation spatially, or by possible ultrasonic induced gradient in a piezoelectric host.²⁵ The i -th and the j -th nanoparticles are separated by a distance $d_{ij} = d_0|i - j|$, with their position denoted by $x_i = d_0(i - 1)$, where $i = 1, 2, \dots, N$. This means that the nanoparticles are equally spaced in a periodical chain which is immersed in a host with dielectric function increasing from ϵ_{left} at the chain's leftmost site to $\epsilon_{\text{left}} + c$ at the rightmost site. Therefore, each spherical nanoparticle acquires an isotropic dipole polarizability

$$\beta_i = \epsilon_2(x_i)a^3 \frac{\epsilon_m(\omega) - \epsilon_2(x_i)}{\epsilon_m(\omega) + 2\epsilon_2(x_i)}. \quad (2)$$

The dipolar resonant frequency is denoted by $\omega_i = \sqrt{\omega_p^2/[1 + 2\epsilon_2(x_i)]}$ which makes the real part of denominator of Eq. (2) zero.² In the coupled dipole approximation, the self-consistent coupling equations of the local fields \mathbf{E}_i around the i -th nanoparticle read,⁶

$$\mathbf{E}_i = \sum_{j \neq i}^N \tilde{\mathbf{T}}(i, j) \cdot (\beta_j \mathbf{E}_j) + \mathbf{E}_i^{(0)}, \quad (i = 1, 2, \dots, N), \quad (3)$$

where $\mathbf{E}_i^{(0)}$ represents the external electric field, and the dipole coupling is given by $\tilde{\mathbf{T}}(i, j) = \mathbf{T}(i, j)/\epsilon_2(x_i)$ where $\mathbf{T}(i, j)$ denotes the near field coupling in vacuum. In Cartesian coordinates (x, y, z) , the (β, γ) components are given by

$$\mathbf{T}_{\beta, \gamma}(i, j) = \frac{3d_{ij, \beta}d_{ij, \gamma} - |\mathbf{d}_{ij}|^2\delta_{\beta, \gamma}}{|\mathbf{d}_{ij}|^5}. \quad (4)$$

Where \mathbf{d}_{ij} represents the vectorial distance with β or γ component $d_{ij,\beta|\gamma}$. After substituting the Drude form into Eq. (2) and eliminating the bulk plasmon frequency ω_p in Eq. (3), we have the following coupled equation of motion for the dipole moments

$$-\omega^2 p_i = -\omega_i^2 p_i + \frac{3\lambda_{(L,T)}\omega_i^2\epsilon_2^2(x_i)}{1 + 2\epsilon_2(x_i)} \left[E_i^{(0)} + \sum_{j \neq i}^N \left(\frac{a}{d_{ij}} \right)^3 \frac{p_j}{\epsilon_2(x_i)} \right], \quad (5)$$

where $\lambda_L = 2$ and $\lambda_T = -1$ are for the cases of longitudinally (i.e., parallel to the chain axis) and transversely polarized $\mathbf{E}_i^{(0)}$ (simply indicated by $E_i^{(0)}$), respectively. In view of the fact that we are concerned with the plasmon waves near the resonant frequency,^{19,20} i.e., $\omega \sim \omega_i$, we have obtained Eq. (5) with the approximation $[\epsilon_2(x_i) - 1]\omega^2 + [2\epsilon_2(x_i) + 1]\omega_i^2 \approx 3\epsilon_2(x_i)\omega_i^2$. Equation (5) captures the main features of the plasmonic coupling between nanoparticles in the PNCs. For example, it shows that the coupling depends on the resonant frequencies, the polarization, and the properties of the metal and the surrounding host, as well as the separations between the particles.⁸

We seek plasmonic eigenmode solutions $\Phi_\alpha(i)$ of Eq. (5) in the absence of the external driving term $E_i^{(0)}$. The results are shown in Fig. 1 for the longitudinal polarization and with parameters listed below: $\epsilon_{\text{left}} = 3.0$, $c = 1.0$, $N = 100$, and $d_0 = 3a$, namely $l = 3a(N - 1)$, where a is the radii of the nanoparticles. In this nanoparticle separation, complications from multipolar interactions are negligible²⁶ and our approximations are quite accurate. It is noteworthy that in the calculations we used the approximation that the dielectric constant of the host around the i -th nanoparticle is homogeneous, e.g., denoted by $\epsilon_2(x_i)$. In this case, we actually have a host dielectric function $\epsilon_2(x_i)$ gradually varying from 3.0 at the left-hand extremity to 4.0 at the right-hand extremity. The solid curve in Fig. 1(a) represents the relationship (i.e., pseudo-dispersion relation) between the coupled plasmon frequency ω and the mode index α for the longitudinal polarization. Longitudinal results for the same PNC within homogenous hosts of dielectric constant $\epsilon_2 = 3.0$ (dash-dotted line) and $\epsilon_2 = 4.0$ (dashed line) are also shown. It is noticed that the presence of a gradient in the host refractive index alters the plasmon (pseudo-) dispersion relation dramatically. This is also signified in the density of states (DOS) $D(\omega) = \sum_\alpha \delta(\omega - \omega_\alpha)/N$, as shown in Fig. 1(b). In detail, the DOS peaks at band-edges of the homogenous host cases (dashed and dash-dotted lines) are shifted toward the Mie dipole plasmon resonant frequencies $\omega_0 = \omega_p/\sqrt{1 + 2\epsilon_2}$, due to the gradient in the host refractive index. More specifically, for the graded host case we studied, there are two peaks in the DOS at around $\omega_{f1} = 0.331\omega_p$ and $\omega_{f2} = 0.364\omega_p$, for near field full couplings (Full) between nanoparticles. The two peaks, however, appear at $\omega_{c1} = 0.337\omega_p$ and $\omega_{c2} = 0.367\omega_p$ if only the nearest-neighboring couplings (NN) are taken into account. These

two peaks in fact correspond to two points of transition between confined modes and extended modes, which is easily seen in Fig. 1(c) showing the inverse participation ration (IPR) of the normal mode,²⁷ as well as directly from the mode patterns (right panels in Fig. 1). Interestingly, the modes outside the frequency range $\omega_{f1} < \omega < \omega_{f2}$ are localized at the two extremities of the PNC, i.e., modes with $\omega > \omega_{f2}$ (high frequencies) are localized at the left-hand side while modes with $\omega < \omega_{f1}$ (low frequencies) are confined at the right-hand side with dramatically increased IPRs. These localization/confinement are clearly shown by the mode patterns in Figs. 1(d) and 1(f). However, normal modes with frequency $\omega_{f1} < \omega < \omega_{f2}$ are extended over the entire PNC [see Fig. 1(e)]. They exhibit IPRs that are near constant as shown in Fig. 1(c).

Intuitively, the existence of localized (confined) modes at the two ends is reasonable in view of the fact that the Mie resonances is lower at the right hand where there is a relatively larger refractive index in the host and higher at the left hand side with a relatively smaller refractive index in the host. But to further understand the localization-delocalization transitions, let us neglect long range interactions and truncate the summation in Eq. (5) up to the nearest neighbors, i.e., consider NN couplings. The resulting coupled plasmon system is similar to a chain of graded coupled harmonic oscillators²⁷ with additional on-site harmonic potentials. In this case, the particle mass m_i , and the strength of the additional harmonic spring U_i are respectively

$$m_i = \frac{1 + 2\epsilon_2(x_i)}{3\lambda\omega_i^2\epsilon_2(x_i)}, \quad (i = 1, 2, \dots, N), \quad (6)$$

$$U_i = \frac{1 + 2\epsilon_2(x_i)}{3\lambda\epsilon_2(x_i)} - 2K_0, \quad (i = 1, 2, \dots, N), \quad (7)$$

where $K_0 = (a/d_0)^3$ is a force constant between adjacent particles that depends on the ratio of the interparticle spacing and the particles radius. Figures 2(a) and 2(b) show m_i and U_i for the case of $d_0 = 3a$ (solid lines) and $d_0 = 2.5a$ (dashed lines) respectively, for $\lambda = \lambda_L = 2$. In this case m_i and U_i are respectively increasing and decreasing functions of i , and for $\lambda = \lambda_T = -1$, they are of the same functions of i (not shown). Illustrating this situation, we can understand that the lower frequency modes are confined at the right side of the chain and higher frequency modes at the left side. The lowest frequency ω_L (i.e., lower bound) of extended modes is the lowest frequency of the homogeneous system with $m_i = m_1$ and $U_i = U_1$ for any i . This frequency ω_L is simply given by

$$\omega_L = \sqrt{U_1/m_1}. \quad (8)$$

Also, the highest frequency ω_H (i.e., upper bound) of extended modes is the highest frequency of

the homogeneous system with $m_i = m_N$ and $U_i = U_N$ for any i . This frequency is given by

$$\omega_H = \sqrt{\frac{4K_0 + U_N}{m_N}}. \quad (9)$$

For parameters $N = 100$, $d_0 = 3a$, $c = 1.0$, $\epsilon_{\text{left}} = 3.0$, and $\lambda_L = 2$, Eqs. (8) and (9) result in $\omega_L = 0.340\omega_p$ and $\omega_H = 0.365\omega_p$, respectively. These are in excellent agreement with the numerical data of nearest-neighboring coupling as shown in Figs. 1(b) and 1(c), where ω_L and ω_H are indicated by the two vertical dashed lines. In Fig. 1(b), they coincide respectively with the two peaks in the DOS with NN couplings, which locate right at the two transition frequencies of $\omega_{c1} = 0.337\omega_p$ and $\omega_{c2} = 0.367\omega_p$.

The analytic results of the transition frequencies given by Eqs. (8) and (9) help to design the passband substantially, although they are for nearest-neighboring coupling. In this sense, we hereby attempt the tunable passband for the longitudinal polarization represented by the analytical forms and confirm it by numerical calculations. The results are demonstrated in Figs. 2(c) and 2(d), where we assume an additional nonlinear host dielectric variation, i.e., $\epsilon_2(x) = (\epsilon_{\text{left}} + cx/l)(1+p)$. Here p indicates the change of dielectric constant due to optical nonlinear effects, i.e., $p = \chi E_{\text{pump}}^2$, where χ is the third order nonlinear susceptibility of the host media and E_{pump} represents a strong pump field. In Fig. 2(c) we plot ω_L (solid lines) and ω_H (dashed lines) as functions of c with $p = 0.0$ for $d_0 = 3a$ and $d_0 = 2.5a$, respectively. We also show the results of ω_{c1} (symbol \square) and ω_{c2} (symbol \bigcirc) extracted from the numerical calculations. The numerical data agree very well with the analytical ones. This figure indicates that with fixed nanoparticle spacing d_0 in the PNC, ω_L keeps relatively constant, while ω_H decreases almost linearly for an increased gradient coefficient c from, say, 0.2 to 1.5. On the other hand, increasing the separation of the nanoparticles, e.g., changing $d_0 = 2.5a$ to $d_0 = 3a$ narrows the passband dramatically, as both ω_L and ω_H approach to the Mie resonant frequency ω_i because the particles become more isolated, that is, the couplings between them are diminished.

Figure 2(d) demonstrates tunability of the passband by nonlinearity effect in the host medium. For example we show the transition frequencies ω_L and ω_H versus p for $d_0 = 3a$ with two different gradient coefficient $c = 0.5$ and $c = 1.0$, respectively. Similarly the numerical data of ω_{c1} (symbol \square) and ω_{c2} (symbol \bigcirc) are compared favorably to the analytical results (curves). It is seen that for increased p , i.e., increased dielectric constant in the graded host, both the low and high transition frequencies are red-shifted. These are ascribed to the fact that the Mie resonant frequency is redshifted when the dielectric constant of the surrounding host is increased. Interestingly, ω_L (ω_{c1})

decreases relatively at the same fashion as ω_H (ω_{c2}) does, varying over a span, e.g., from around $0.35\omega_p$ to a extremely low frequency. Admittedly, it is hard to achieve such a large nonlinear modulation, for example, for $p > 1.0$. However, a relatively small modulation in the host dielectric nonlinearity, e.g., from $p = 0.0$ to $p = 0.5$ still results a desirable tuning of ω_L and ω_H . We believe these results can find potential applications of dynamical switching in plasmonics. The pump field may also induce a nonlinearity in the metallic particles. However, the nonlinearity in host is assumed to be larger, resulting in a graded polarizability along the chain. Finally, the results for the transverse modes ($\lambda = -1$) are quite similar to those of the longitudinal modes ($\lambda = 2$) presented here.

In summary, we propose the use of a gradient dielectric host to achieve the precise confinement of electromagnetic fields in plasmonic nanoparticle chains. It is demonstrated that the coupled surface plasmons in these systems become easily tunable between confined modes and extended modes. We offer an interpretation of the transition mechanism by mapping the problem onto a graded coupled harmonic oscillators. In addition to possible operation for plasmonic switching, these systems may be also of interest for applications such as surface-enhanced Raman scattering or biosensing.

This work was supported in part by the RGC Earmarked Grant of the Hong Kong SAR Government (K.W.Y.), and in part by a Grant-in-Aid for Scientific Research from Japan Society for the Promotion of Science (No. 16360044).

-
- ¹ H. Raether, *Surface Plasmons* (Springer-Verlag, Berlin, 1988).
 - ² N. Zheludev and V. Shalaev, (eds.), *J. Opt. A: Pure Appl. Opt.* **7**, S1 (2005), the special issue on nanostructured optical meta-materials: beyond photonic bandgap effects.
 - ³ A. V. Zayats and I. I. Smolyaninov, *J. Opt. A: Pure Appl. Opt.* **5**, S16 (2003).
 - ⁴ W. L. Barnes, A. Dereux, and T. W. Ebbesen, *Nature (London)* **424**, 824 (2003).
 - ⁵ E. Hutter and J. H. Fendler, *Adv. Mater.* **19**, 1685 (2004).
 - ⁶ C. Girard, *Rep. Prog. Phys.* **68**, 1883 (2005).
 - ⁷ A. V. Zayats, I. I. Smolyaninov, and A. A. Maradudin, *Phys. Rep.* **408**, 131 (2005).
 - ⁸ S. A. Maier and H. A. Atwater, *J. Appl. Phys.* **98**, 011101 (2005).

- ⁹ D. K. Gramotnev and D. F. P. Pile, Appl. Phys. Lett. **85**, 6323 (2004).
- ¹⁰ D. F. P. Pile, T. Ogawa, D. K. Gramotnev, T. Okamoto, M. Haraguchi, M. Fukui, and S. Matsuo, Appl. Phys. Lett. **87**, 061106 (2005).
- ¹¹ S. Feng, J. M. Elson, and P. L. Overfelt, Opt. Express **13**, 4113 (2005).
- ¹² M. Hochberg, T. Baehr-Jones, C. Walker, and A. Scherer, Optics Express **12**, 5481 (2004).
- ¹³ A. Karalis, E. Lidorikis, M. Ibanescu, J. D. Joannopoulos, and M. Soljčić, Phys. Rev. Lett. **95**, 063901 (2005).
- ¹⁴ B. Lamprecht, J. R. Krenn, G. Schider, H. Ditlbacher, M. Salerno, N. Felidj, A. Leitner, F. R. Aussenegg, and J. C. Weeber, Appl. Phys. Lett. **79**, 51 (2001).
- ¹⁵ M. I. Stockman, Phys. Rev. Lett. **93**, 137404 (2004).
- ¹⁶ K. Li, M. I. Stockman, and D. J. Bergman, Phys. Rev. Lett. **91**, 227402 (2003).
- ¹⁷ D. F. P. Pile and D. K. Gramotnev, Appl. Phys. Lett. **86**, 161101 (2005).
- ¹⁸ T. A. Kelf, Y. Sugawara, J. J. Baumberg, M. Abdelsalam and P. N. Bartlett, Phys. Rev. Lett. **95**, 116802 (2005).
- ¹⁹ S. Y. Park and D. Stroud, Phys. Rev. B **69**, 125418 (2004).
- ²⁰ M. L. Brongersma, J. W. Hartman, and H. A. Atwater, Phys. Rev. B **62**, R16356 (2000).
- ²¹ M. I. Stockman, S. V. Faleev, and D. J. Bergman, Phys. Rev. Lett. **87**, 167401 (2001).
- ²² D. A. Genov and V. M. Shalaev, and A. K. Sarychev, Phys. Rev. B **72**, 113102 (2005).
- ²³ W. Nomura, M. Ohtsu, and T. Yatsui, Appl. Phys. Lett. **86**, 181108 (2005).
- ²⁴ P. Ghenuche, R. Quidant, and G. Badenes, Opt. Lett. **30**, 1882 (2005).
- ²⁵ F. Silly and M. R. Castell, Appl. Phys. Lett. **87**, 213107 (2005).
- ²⁶ J. J. Xiao, J. P. Huang, and K. W. Yu, Phys. Rev. B **71**, 045404 (2005).
- ²⁷ J. J. Xiao, K. Yakubo, and K. W. Yu, Phys. Rev. B **73**, 054201 (2006).

Figure Captions

FIG. 1: (Color online) (a) Pseudo-dispersion relations for full coupling. Those for cases of homogeneous host with $\epsilon_2 = 3.0$ (dash-dotted line) and $\epsilon_2 = 4.0$ (dashed line) can be regarded as the usual dispersion relations. (b) Density of states (DOS) versus coupled plasmon mode frequency for the full coupling. The line with circles represent results of graded case for nearest-neighboring coupling. (c) Inverse participation ratio (IPR) versus plasmon mode frequency. (d) Typical excitation in low frequency regime ($\omega = 0.315\omega_p$). (e) Typical excitation near the resonant frequency ($\omega = 0.353\omega_p$). (f) Typical excitation at high frequency ($\omega = 0.390\omega_p$).

FIG. 2: (Color online) (a) Effective mass m_i and (b) on-site potential U_i for $d_0 = 3a$ and $d_0 = 2.5a$ with $c = 1.0$ and $p = 0.0$. (c) Analytical (curves) and numerical (symbols) transition frequencies ω_L (ω_H) and ω_{c1} (ω_{c2}) versus the host gradient coefficient c without nonlinearity ($p = 0.0$) for different nanoparticle distances d_0 . (d) Analytical (curves) and numerical (symbols) transition frequencies versus nonlinearity (pump field) modulation in the host medium, with $d_0 = 3a$ for different host gradient coefficient $c = 0.5$ and $c = 1.0$, respectively.

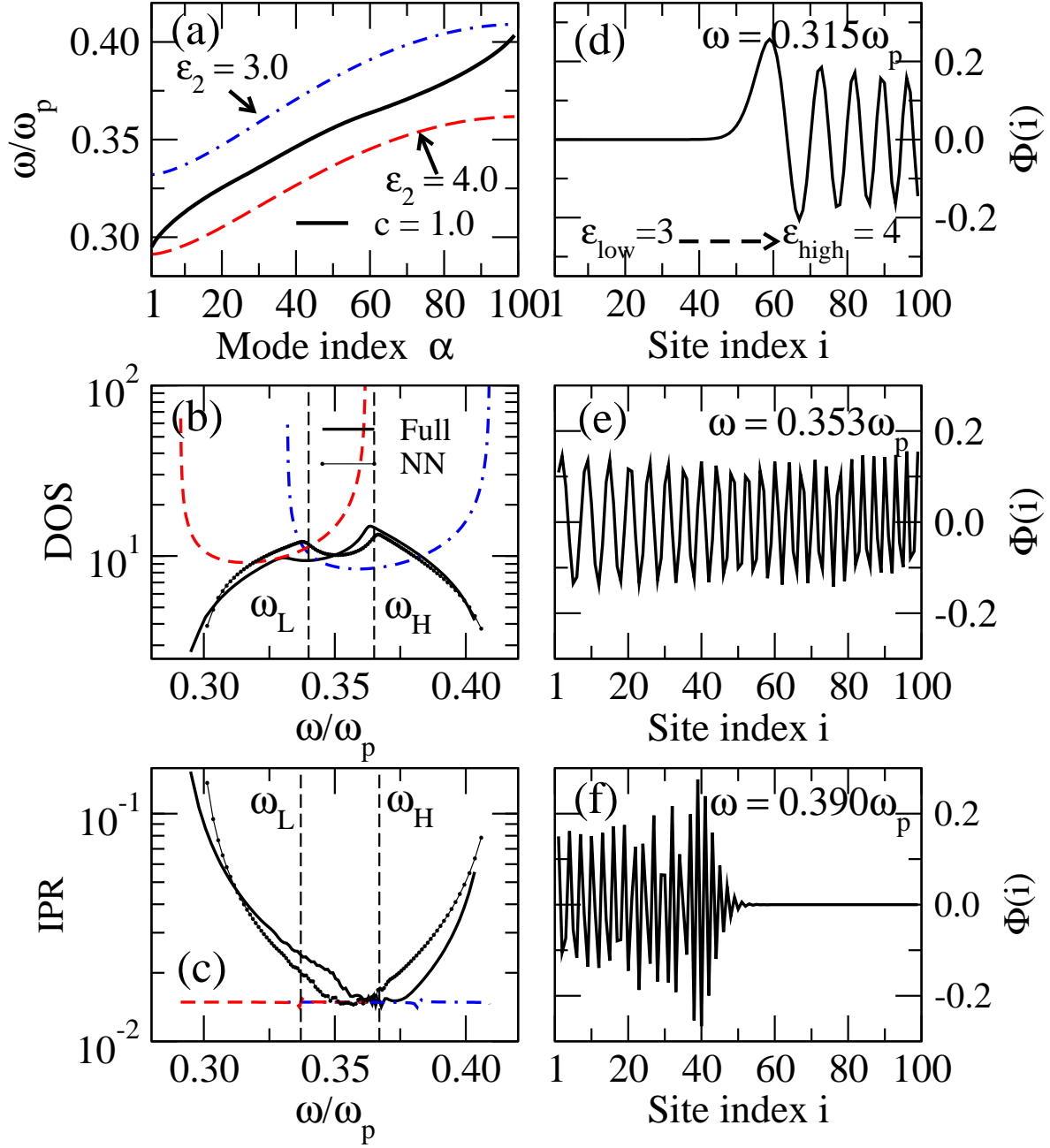


Fig.1./Xiao, Yakubo, and Yu

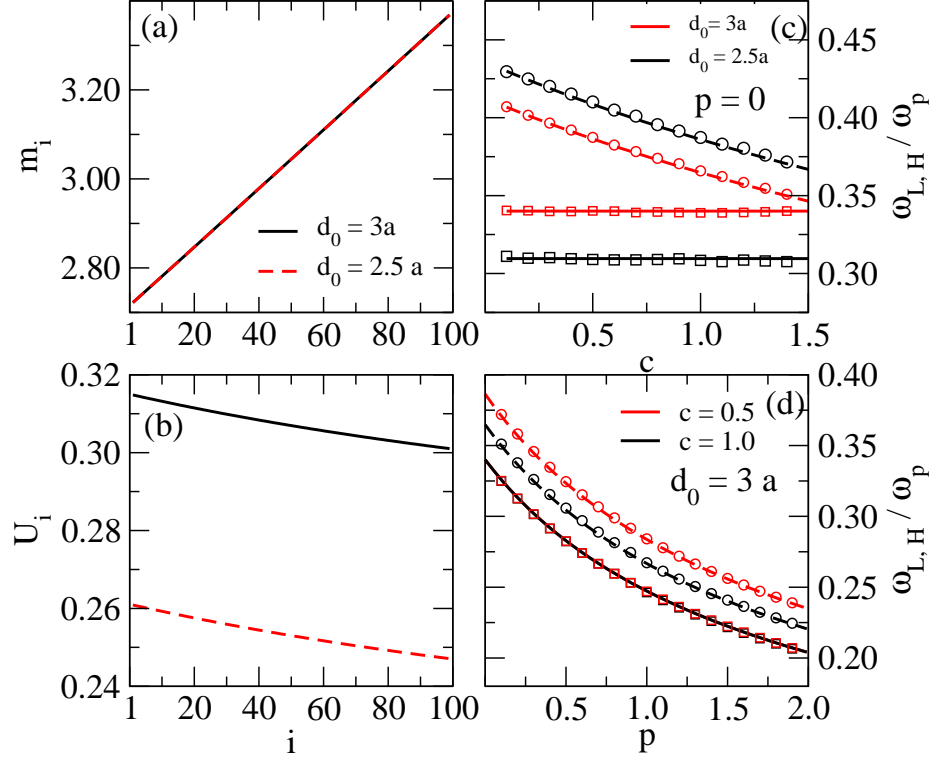


Fig.2./Xiao, Yakubo, and Yu